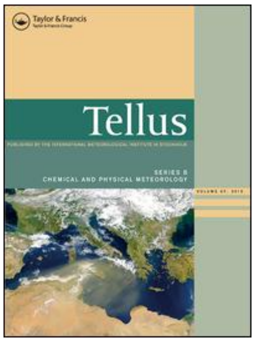

Tellus B: Chemical and Physical Meteorology

ISSN: (Print) 1600-0889 (Online) Journal homepage: http://www.tandfonline.com/loi/zelb20

Size-dependent aerosol activation at the high-alpine site Jungfraujoch (3580 m asl)

S. Henning, E. Weingartner, S. Schmidt, M. Wendisch, H. W. Gäggeler & U. Baltensperger

To cite this article: S. Henning, E. Weingartner, S. Schmidt, M. Wendisch, H. W. Gäggeler & U. Baltensperger (2002) Size-dependent aerosol activation at the high-alpine site Jungfraujoch (3580 m asl), Tellus B: Chemical and Physical Meteorology, 54:1, 82-95, DOI: 10.3402/tellusb.v54i1.16650

To link to this article: https://doi.org/10.3402/tellusb.v54i1.16650

Published online: 15 Dec 2016.

Tellus (2002), 54B, 82–95
Printed in UK. All rights reserved

TELLUS
ISSN 0280–6509

Size-dependent aerosol activation at the high-alpine site Jungfraujoch (3580 m asl)

By S. HENNING[1], E. WEINGARTNER[1], S. SCHMIDT[2], M. WENDISCH[2], H. W. GÄGGELER[1,3] and U. BALTENSPERGER[1]*, [1]*Paul Scherrer Institut (PSI), CH-5232 Villigen PSI, Switzerland;* [2]*Institute for Tropospheric Research (IfT), DE-04318 Leipzig, Germany;* [3]*Department of Chemistry and Biochemistry, University of Bern, CH-3012 Bern, Switzerland*

(Manuscript received 16 March 2001; in final form 4 October 2001)

ABSTRACT

Microphysical and chemical aerosol properties and their influence on cloud formation were studied in a field campaign at the high-alpine site Jungfraujoch (JFJ, 3580 m asl). Due to its altitude, this site is suitable for ground-based in-cloud measurements, with a high cloud frequency of 40%. Dry total and interstitial aerosol size distributions [18 nm < particle diameter (D_p) < 800 nm] were determined with a time resolution of 6 min. A forward scattering spectrometer probe (FSSP-100) measured the cloud droplet size distribution, and a particle volume monitor (PVM-100) was used to measure liquid water content (*LWC*). In addition, the aerosol chemical composition (major soluble ions) was determined in two size classes (total and submicron particles). Agreement within the range of measurement uncertainties was observed between the droplet number concentrations derived from the aerosol size distribution measurements (total minus interstitial) and those measured by the FSSP. The observed particle diameter at 50% activation (D_{50}) was typically around 100 nm for $LWC \geqslant 0.15$ g m^{-3}. Below this value, D_{50} increased with decreasing *LWC*. A dependence of D_{50} on the accumulation mode ($D_p > 100$ nm) number concentration ($N_{tot,D_p>100}$) was only found for concentrations less than 100 cm^{-3}. For higher values of $N_{tot,D_p>100}$ the D_{50} remained constant. Furthermore, a decrease of the effective radius of cloud droplets (R_{eff}) with increasing $N_{tot,D_p>100}$ was observed, providing experimental evidence for the microphysical relation predicted by the Twomey effect. A modified Köhler model was used to quantify the critical supersaturation for the aerosol observed at the JFJ. Ambient supersaturations were determined from the derived supersaturation curve and the calculated D_{50}. As an example, a critical supersaturation of 0.2% was found for 100 nm particles.

1. Introduction

Atmospheric aerosols play an important role in cloud formation. The homogeneous nucleation of water droplets requires a supersaturation of several hundred percent (Pruppacher and Klett, 1980). This never occurs in nature due to the sufficient concentration of atmospheric aerosols that act as cloud condensation nuclei (CCN) at much lower supersaturations. The relative humidity (*RH*) of an air parcel increases as it is lifted vertically in the atmosphere. At the deliquescence point, which depends on the chemical composition [e.g. $RH = 82\%$ for ammonium sulfate at $-10\,^{\circ}$C (Onasch et al., 1999)], the water-soluble components of the CCN dissolve. With continued increase in *RH*, the CCN grow through the addition of water. Above saturation, if a CCN reaches its critical diameter it will continue to grow as long as the parcel remains supersaturated, even if the

* Corresponding author.
e-mail: urs.baltensperger@psi.ch

supersaturation falls below the particle's critical diameter. This critical diameter depends on the particle chemical composition and its dry size. Particles that do not reach their critical diameter are not activated and form the interstitial aerosol population.

This particle activation process is of special interest with regard to cloud evolution and hence determines cloud optical properties, which have an influence on the Earth's energy budget. With increasing aerosol number concentrations, caused e.g. by human activity, more particles are available for activation, leading to more and smaller water droplets. As a consequence, and under the assumption that the cloud liquid water content (*LWC*) stays constant, the cloud albedo will increase and so will the backscattering of solar radiation (Twomey, 1974; 1977). This connection is known as the first indirect aerosol effect, while the suppression of precipitation is known as the second indirect aerosol effect. Both effects are widely discussed in the scientific community; they nevertheless remain poorly understood and quantified (IPCC, 2001).

Several experimental approaches have been used to understand the aerosol activation process, such as a comparison of the properties of: (a) cloud droplets with pre-cloud aerosol (Choularton et al., 1997), (b) interstitial aerosol with pre-cloud aerosol (Martinsson et al., 1999; Svenningsson et al., 1997), (c) airborne studies in- and below-cloud (Gillani et al., 1995; Leaitch et al., 1996) and (d) cloud droplets with the in-cloud interstitial aerosol (Schwarzenboeck et al., 2000).

In this study a different approach was adopted. Interstitial and total aerosol (i.e., the sum of particles that were activated or scavenged plus those that remained interstitial) were measured with the same experimental set-up alternating every 6 min. Thus, a quasi-parallel measurement of total and interstitial aerosol was realized without assuming information on the air parcel trajectory, as is the case for the approaches in (a), (b) and (c). Due to logistical considerations, cloud experiments are preferably conducted at ground-based locations. Results reported in this study were performed at the high-alpine site Jungfraujoch (JFJ, 3580 m asl), which experiences in-cloud conditions about 40% of the time (annual average) (Baltensperger et al., 1998). The presented data were obtained during a dedicated field campaign lasting from 24 July to 10 August 2000.

2. Experimental

Aerosol number size distributions of the total and the interstitial aerosol were measured with a scanning mobility particle sizer (SMPS, particle diameter $D_p = 18$–800 nm). A forward scattering spectrometer probe (FSSP-100, Particle Measuring Systems Inc., USA) was operated to detect the cloud droplet size distribution, and a particle volume monitor (PVM-100, Gerber Scientific Inc, USA) measured the *LWC*. In addition, measurements of the chemical aerosol composition were performed in two size classes [total suspended particulate matter (TSP) and particles with an aerodynamic diameter less than 1 μm (PM_1)], of the total aerosol. In addition, data from other instruments continuously operated at the JFJ in the framework of the Global Atmosphere Watch (GAW) Program (Nyeki et al., 1998) were available, as well as data from continuous meteorological measurements (wind direction, wind velocity, air pressure, air temperature, relative humidity, solar radiation) from the Swiss Meteorological Institute (SMI) and the mass of total suspended particulate matter (TSP) from the Swiss National Monitoring Network for Air Pollutants (NABEL).

2.1. *Description of the JFJ measurement site*

The high-alpine research station JFJ (3580 m asl; 46°33′N, 7°59′E, Switzerland) is part of the GAW Program of the World Meteorological Organization, since it is an ideal site to investigate the chemistry and physics of the free troposphere above a continental region. More information about the site is found in Baltensperger et al. (1997).

2.2. *Meteorological conditions*

The general weather situation was quite variable during the measuring campaign. Several fronts passed over the region, while high-pressure systems were experienced on some days. At the end of July a weak cold front crossed the Alps followed by an occlusion. Maritime subpolar air and later maritime subtropical air was transported towards the Alps. Thereafter, a high-pressure system advected maritime subpolar air masses to the JFJ until 3 August. On the backside of the high, subtropical air was advected. The following cold front and the deep pressure system brought maritime and altered subpolar air again. The air masses had similar properties, while several fronts crossed the area by 9 August. On 10 August a new strong high-pressure system influenced the Alps in connection with subtropical air. The observed cloud types were Stratocumulus and Cumulus, as determined from the general weather situation, eye observations and satellite records.

The median temperature for the whole campaign was $-1.4\,^{\circ}$C, with a range of -6.5 to $4.6\,^{\circ}$C (Table 1). During cloudy conditions, which occurred a total of 136 h (30% of the time) the median was slightly lower with $-3.5\,^{\circ}$C. At this temperature the majority of clouds consisted of supercooled cloud droplets. The median wind speed was $8.6\ \mathrm{m\,s^{-1}}$ for all conditions and $11.4\ \mathrm{m\,s^{-1}}$ for clouds only. As a result of the local JFJ orography, the prevailing wind direction was either North-West or South-East. North-westerly winds occurred with a 67% frequency when averaged over the whole campaign, but increased to 82% when considering only cloudy conditions. The median liquid water content for all recorded clouds was $0.23\ \mathrm{g\,m^{-3}}$.

2.3. *The inlet systems*

Aerosol particles were sampled from two different inlet systems. The total aerosol inlet is heated to $20\,^{\circ}$C and is designed to evaporate all cloud droplets at a very early stage of the sampling process. Calculations for this set-up showed that activated droplets smaller than 40 μm can be sampled up to a wind speed of $20\ \mathrm{m\,s^{-1}}$ (Weingartner et al., 1999). The total sample thus consists of aerosols activated to cloud droplets, aerosols scavenged by droplets, and inactivated (interstitial) aerosols. The second inlet system was designed to only sample interstitial aerosols, using an aerodynamic size discriminator (Round Jet Impactor) operating at ambient temperature (i.e. without any heating). This device is a conventional impactor where particles larger than the cut-off size are unable to follow the airflow streamlines and hence impact onto a plate. The cut-off size is given by the slit width of the impactor and the flow rate. In our setup an impactor with a cut-off diameter at 5 μm was used as the interstitial aerosol inlet. Once a day sampling was interrupted and the inlet was cleaned and dried.

2.4. *Measurement of aerosol size distributions*

The atmospheric aerosol was fed into the building (indoor $T = 20$–$30\,^{\circ}$C, $RH < 10\%$) from either the total inlet or the interstitial inlet using two pinch-valves, and then on to a single SMPS (scanning mobility particle sizer) system for measurement of the size distribution. The SMPS consisted of a differential mobility analyzer (DMA, TSI 3934), a bipolar charger to obtain charge equilibrium (krypton source, ^{85}Kr) and a condensation particle counter (CPC, TSI 3022A). The poly- and monodisperse aerosol flows were $0.3\ \mathrm{l\,min^{-1}}$ while sheath and excess air flows ($3\ \mathrm{l\,min^{-1}}$) were operated in a closed-loop system. The excess air outlet of the DMA was fixed to the vacuum side of the pump, while the air exiting the pump was cleaned from particles by a filter and used as sheath air. The flow was held constant by a critical orifice positioned before the pump.

With this set-up the dry aerosol size distribution from $D_p = 18$–800 nm was measured at an average ambient pressure of 650 hPa. Scanning was per-

Table 1. *Overview over weather conditions during the measuring campaign*

	All conditions (455 h)			Clouds only (136 h)		
	10% perc.	median	90% perc.	10% perc.	median	90% perc
Temperature (°C)	-4.4	-1.4	1.6	-5.5	-3.5	-1.2
Wind speed[a] ($\mathrm{m\,s^{-1}}$)	4.3	8.6	15.6	5.6	11.4	18.1
LWC ($\mathrm{g\,m^{-3}}$)	0.00	0.01	0.28	0.11	0.23	0.43

[a] Main wind directions: 67% NW, 13% SE and 82% NW, 5% SE for all times and clouds only, respectively.

formed in logarithmically equidistant steps with a time resolution of about 6 min per scan (300 s up scan time, 10 s down scan and 60 s wait time while the inlet line was switched, resulting in a scanning velocity of $d \log D/dt = 5.7 \times 10^{-3}\,s^{-1}$). With this scanning velocity no deformation of the size distribution occurs (Weingartner et al., 2002). The scanning time was synchronized with the time of the pinch valve. For further data processing 1-h averages of the interstitial and total particle size distributions were calculated.

2.5. *Calibration of the SMPS system*

To make sure that the aerosol size distribution was not biased by diffusion and impaction losses in the pinch valves, tests with monodisperse latex spheres (nominal diameters of 91 ± 6 nm and 550 ± 5 nm) were performed. A latex solution was nebulized, and the droplets were dried in a diffusion dryer. The particle number concentrations of the monodisperse size distributions were measured before and after passing the pinch valve. The calculated deviations of the particle number concentration between the different lines were of the same order of magnitude as the inter-variance of the original aerosol size distributions. For the 91 nm latex spheres the deviation at the maximum of the distribution was 9% and the variance was calculated to be 7%, while for the 550 nm latex spheres values of 6% and 5% were found, respectively. Based on these results the influence of the two-way pinch valve on particles losses can be neglected.

This experimental setup was also used to check the voltage to diameter adjustment and the delay time of the SMPS. The measured particle size distributions were fitted with a lognormal function. For the 91 nm polystyrene particles a diameter of 90 nm with a half-width of 8 nm was detected. A diameter of 556 nm with a corresponding half-width of 80 nm was observed for the 550 nm spheres.

With a slightly different experimental set-up, where a particle filter was included in one line and ambient air was measured in the other path, it was shown that the waiting time of 60 s between two scans was sufficient to flush all particles from the previous scan out of the inlet system.

2.6. *Instrumentation for measuring cloud microphysics*

A PVM-100 (Gerber, 1991) was used to measure total *LWC* during the experiment. It measures the light scattered by a cloud droplet population exposed to a laser beam and relates it to the *LWC*. It was situated outside the building on the rail of the upper platform of the building. The optics of the PVM-100 were cleaned just before the experiment, secondary calibration was conducted regularly (typically every cloud-free day) as suggested by the manufacturer.

The FSSP-100, situated 2 m away from the PVM-100, was used for measuring cloud droplet size distributions in the droplet diameter range between either 4.5 and 30 μm or 6.3 and 62 μm. In difference to the PVM, the FSSP sizes the single droplets one by one. The droplets are passed through a laser beam corresponding to the amount of light scattered by the drops in the forward direction. A description of this probe can be found in Knollenberg (1981). For ground-based measurements, air is actively sucked into the sampling tube to provide a constant droplet stream and a well defined sample volume.

Dye and Baumgardner (1984) and Cerni (1983) report on systematic errors of the instrument which can be divided into two types: (a) under- or oversizing of droplets due to varying opto-electronical setup, and (b) counting losses caused by coincidences (when there are two or more droplets simultaneously in the laser beam) and by the electronic dead-time. To correct for sizing uncertainties, calibration with monodisperse glass beads was conducted before, during, and after the campaign. Counting losses were compensated by multiplying the measured concentrations with the half-empirical correction factor $1/(1 - mA)$ proposed by Baumgardner et al. (1985), where A is the measured activity, i.e. the fraction of time the probe was active processing droplet data. The parameter m was considered to be constant and set to 0.73 as proposed by the manufacturer. In addition, the concentration was corrected for a varying velocity acceptance ratio (Wendisch, 1998), which was simultaneously measured. A comparison of different correction schemes for concentration measurements with the FSSP is given by Brenguier (1989).

Wind ramming (Choularton et al., 1986) alters the droplet velocity, and hence changes the sample volume and the droplet concentration. However, this possible bias could not be corrected as wind sensors next to the instrument were not available. Laser beam inhomogeneities (Baumgardner and Spowart, 1990) which systematically broaden the measured droplet size distribution measured with an FSSP (Wendisch et al., 1996), were not considered because the laser beam cross section intensity profile is not sufficiently stable.

The droplet number concentration N_i ($i = 1, \ldots, 15$, denotes the channel number) for each of the FSSP size channels is obtained by dividing the raw counts in the 15 size classes by the sampled air volume. The total droplet concentration N_D is obtained by summing up over all size classes. The *LWC* and the effective radius (R_{eff}) are defined as:

$$LWC = \frac{\pi}{6} \rho_w \sum_{i=1}^{15} N_i D_i^3 \quad (1)$$

$$R_{eff} = \frac{1}{2} \sum_{i=1}^{15} N_i D_i^3 \bigg/ \sum_{i=1}^{15} N_i D_i^2 \quad (2)$$

where ρ_w is the density of water and D_i are the center droplet diameters in each size channel i, attributed by the size calibration. The corrected droplet size distribution is obtained by dividing the droplet number concentration N_i by the width of the respective size channel.

The *LWC*, calculated from the corrected FSSP data [eq. (1)], were compared to the *LWC* directly measured by the PVM, which revealed the following correlation equation (correlation coefficient R^2 of 0.81):

$$LWC(FSSP) = LWC(PVM) \times 1.484 - 0.009 \text{ g m}^{-3}. \quad (3)$$

The systematic underestimation of the *LWC* by the PVM may be a result of decreasing sensitivity of the PVM with increasing droplet diameter as reported by Arends et al. (1992), Wendisch et al. (1998) and Wendisch (1998), but may also be explained by a varying sample volume of the FSSP. Wind tunnel tests of the airborne version of the PVM (the PVM-100A) have also shown a decreasing sensitivity of the PVM with increasing droplet diameter (Wendisch et al., 2001). In the results section the *LWC* measured by the PVM was used, if not mentioned otherwise.

2.7. *Chemical aerosol analysis*

In addition to aerosol physical properties, filter samples in two size classes (total suspended particles, TSP and particles with $D_p < 1$ µm, PM_1) for aerosol chemical analysis were obtained at the total aerosol inlet. The cut-off of 1 µm was achieved by using the first 5 stages of the 12-stage impactor developed by Maenhaut et al. (1996). The flow was held constant at 11 l min^{-1} by a mass flow controller, which yielded the desired cut-off diameter of 1 µm for the PM_1 line. The aerosol was sampled on filter packs consisting of a Teflon (Sartorius, Microfilter PTFE; 1.2 µm pore diameter) and a nylon (Gelman, Nylasorb, 1.0 µm pore diameter) filter. This type of set-up was chosen to catch semi-volatile nitrate aerosol material on the nylon filter, which evaporated from the Teflon filter. The sampling interval was 24 h during the whole campaign.

The samples were stored at temperatures of about −8 °C and were analyzed for major anions and cations (soluble portion) by ion chromatography shortly after the campaign.

3. Results and discussion

3.1. *Size distribution of total and interstitial aerosol*

The influence of clouds on the aerosol size distribution for a selected time period (6–9 August 2000) is shown in Fig. 1. The measured particle size distributions (Fig. 1a–c) are plotted as contour plots of 1-h averages with concentrations of $dN/d\log(D_p)$ or $dN/d\log(D_D)$ versus time. In (a) the total aerosol size distribution is shown while in (b) the interstitial aerosol size distribution is plotted. The shape of the particle size distribution of the total aerosol is typically bimodal for the JFJ aerosol (Weingartner et al., 1999). During cloudless periods it is virtually identical to that of the interstitial distribution. During in-cloud periods aerosol particles are activated to cloud droplets and thus removed from the interstitial particle size distribution. This is illustrated in Fig. 1d, where the difference in the number concentration ($N_{tot} - N_{int}$, with N_{tot} being the total particle number concentration of scavenged plus interstitial aerosol and N_{int} the total number of interstitial aerosol particles) between both inlet

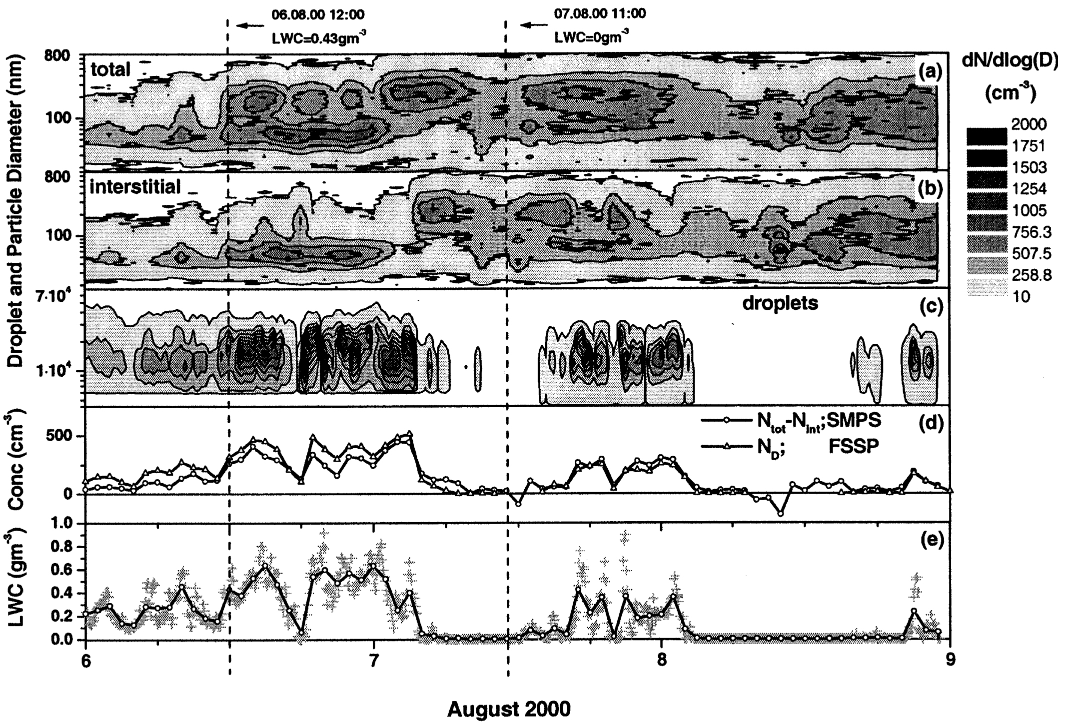

Fig. 1. Contour plots of the total (a) and interstitial (b) aerosol size distributions, droplet size distribution (c), droplet number concentration and the difference between total and interstitial aerosol number concentration (d), and the liquid water content of the ambient air (e). The presented data for the period 6–9 August 2000 0:00 LST are 1-h averages (a, b, d, e), 20-min averages (c), while the crosses in (e) are 5-min values.

systems is plotted. These values should correspond with the droplet number concentration N_D. Only insignificant differences in the number concentrations are found for cloudless periods, and values up to 500 cm^{-3} for thick clouds (*LWC* plotted in Fig. 1e), which is a typical droplet number concentration for this cloud type (Martinsson et al., 1999; Wendisch, 1998). In Fig. 1c the droplet size distribution measured by the FSSP is shown as a contour plot of 20 min average values. Data were obtained in the FSSP size range 1 ($6.3 < D_D < 62$ μm) from 6–7 August, and range 2 ($4.5 < D_D < 30$ μm) after 7 August.

In Fig. 1d the droplet number concentration measured by the FSSP is also plotted. The concentrations calculated from the SMPS differences and the directly measured droplet number concentrations agree well for the plotted example as well as over the whole 3-week measuring period. The correlation coefficient (R^2) is 0.85 for the whole period and the relation can be described as:

$$C(N_{\text{tot}} - N_{\text{int}}) = C(FSSP) \times 0.83 - 15.3\ \text{cm}^{-3}. \tag{4}$$

This good agreement is an experimental confirmation of the theoretical calculation (Weingartner et al., 1999) showing that the total aerosol inlet samples the majority of cloud droplets under the prevailing conditions. Since the SMPS data vary between over- and underestimation of the droplet number concentration, the difference between both instruments does not appear to be systematic and may be caused by the sensitivity of the FSSP to higher wind speed or to a variation in the droplet spectra.

As typical examples of an in-cloud and cloudless period the data from the two marked dates in Fig. 1 are shown in more detail in Fig. 2, where the 1-h averages of the total and interstitial aerosol size distributions are plotted. In Fig. 2, the cloud

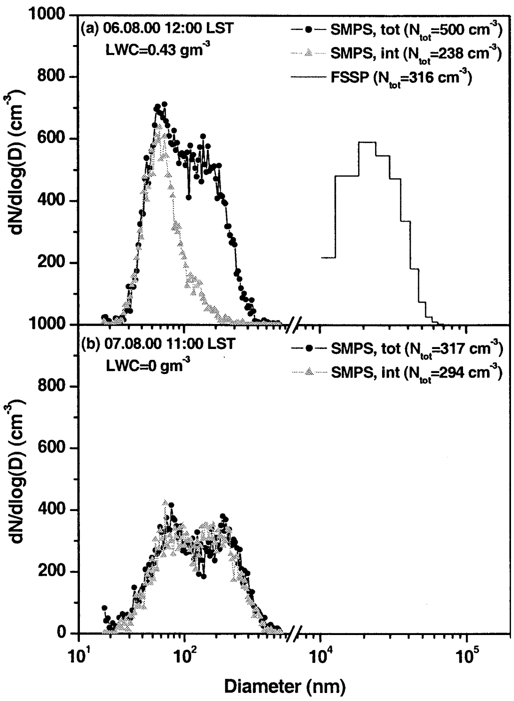

Fig. 2. Averaged size distributions of the total (circles) and interstitial (up triangles) aerosol during a cloud event (a) and without cloud (b). In (a) the cloud droplet size distribution is also plotted. The given *LWC* values were measured by the PVM.

droplet size distribution is also given. At the total aerosol inlet, Aitken ($20 < D_p < 100$ nm), and accumulation mode particles ($100 < D_p < 800$ nm) were observed in both cases, with mean diameters of 65 and 150 nm, respectively, for the cloud event, and 90 and 200 nm, respectively, for the cloudless period. The corresponding interstitial size distributions indicate complete scavenging of the accumulation mode aerosol during the cloud passage, while the Aitken mode remained essentially unactivated. This is also seen in the number concentrations, with 500 cm^{-3} for the total and 238 cm^{-3} for the interstitial aerosol. The nearly complete activation of the accumulation mode leads to the conclusion that the ambient aerosol at the JFJ is mostly internally mixed with respect to its activation behavior. The droplet number concentration of 316 cm^{-3}, calculated from the FSSP data, also shows reasonable agreement with a value of 262 cm^{-3}, being the difference of the total and interstitial aerosol concentrations.

3.2. Calculation of the scavenging ratio

To compare our data with previous results, a first analysis is performed for the activated fraction of particles with a diameter larger than a certain threshold, x:

$$F_{N,D_p>x} = \frac{(N_{\mathrm{tot},D_p>x} - N_{\mathrm{int},D_p>x})}{N_{\mathrm{tot},D_p>x}}, \tag{5}$$

where $N_{\mathrm{tot},D_p>x}$ is the total number concentration of particles with $D_p > x$ nm and $N_{\mathrm{int},D_p>x}$ is the total number of interstitial aerosol particles above the threshold.

Median values of $F_{N,D_p>x}$ of 0.49, 0.65, 0.7, 0.8, 0.83 were observed for $x = 50$, 80, 100, 170 and 300 nm, respectively. A mean activated fraction of $\bar{F}_{N,D_p>170\,\mathrm{nm}} = 0.7$ (standard deviation 0.3) is found over all in-cloud periods, which is comparable to Gillani et al. (1995), where values between 0.19 and 0.96 are given, and Baltensperger et al. (1998) with 0.48 for $x = 100$ nm and 0.83 for $x = 200$ nm.

From the measured size distributions of the total and interstitial aerosols the size-resolved scavenged fraction for each particle diameter F_N (D_p) is calculated in the following way:

$$F_N(D_p) = \frac{[N_{\mathrm{tot}}(D_p) - N_{\mathrm{int}}(D_p)]}{N_{\mathrm{tot}}(D_p)}. \tag{6}$$

The calculated scavenging ratio as a function of D_p for the example from Fig. 2 is shown in Fig. 3. The activated aerosol fraction clearly increases with increasing diameter, approaching 1 for $D_p \geqslant 250$ nm. Significant scatter at the lower end of the size distribution is due to low particle number concentrations in this size range. The diameter where 50% of the aerosol particles are scavenged is called D_{50}. In the presented example this diameter is about 100 nm. To calculate D_{50}, the data were empirically fitted using the hyperbolic tangent function

$$F_N(D_p) = \frac{[1 + \tanh(a \times (D_p - D_{50})]}{2}. \tag{7}$$

Due to the scatter of the data points at the lower end, only data for particle diameters larger that 30 nm were included into the fitting process. From these fits, D_{50} was calculated for all 1-h averages of the campaign. The results are plotted in Fig. 4 along with the *LWC* (measured by the PVM) of the cloud over the whole measuring

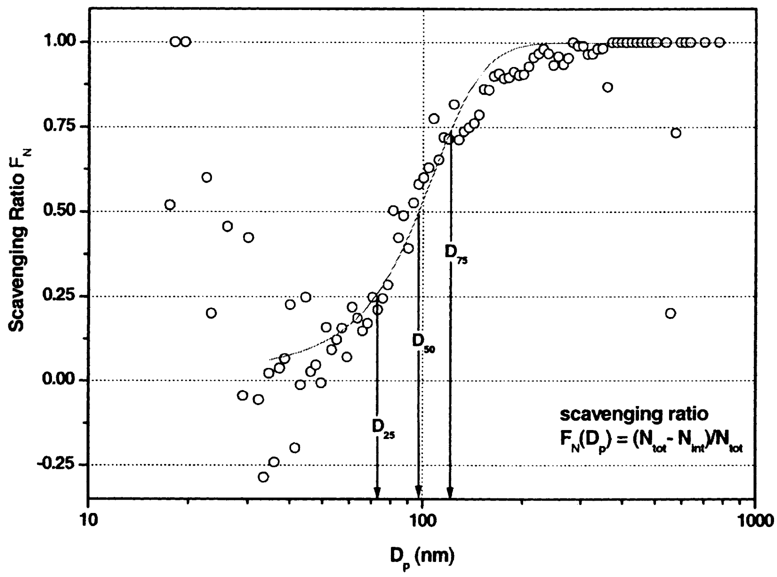

Fig. 3. Calculated scavenging ratio for the cloud event from Fig. 2a. The solid line is a fit with a hyperbolic tangent, and the diameters of 25%, 50% and 75% activation are marked.

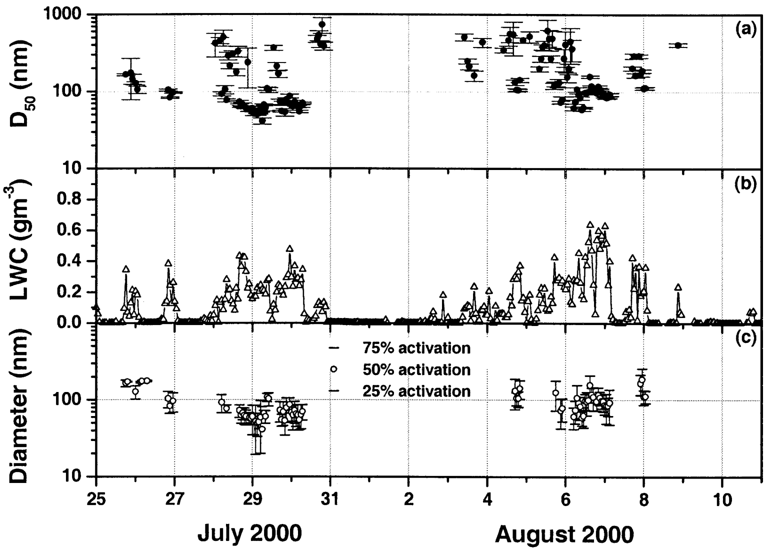

Fig. 4. Diameter of 50% scavenging (a) in comparison with the liquid water content (b) over the whole measuring period. As parameter of the steepness of the activation the diameters of 25% and 75% activation are added as bars (c). The activation diameter is only plotted for *LWC* 15th percentile >0.02 g m^{-3}.

campaign. Due to the high variability of clouds, an activation diameter is only shown for stable conditions, i.e., when the PVM indicated a cloud with an *LWC* larger than 0.02 g m^{-3} during 85% of the time (i.e., *LWC* 15th percentile >0.02 g m^{-3}). Due to the variability of the cloud also within 1 min, this criterion might not be able to completely eliminate all cloud-free conditions. However, if there had been cloud-free conditions for a substantial fraction of time, this would result in a decrease of the activated fraction also for the largest particles. The median of the activated fraction for particles $D_p > 500$ nm was 0.91 for conditions with $LWC > 0.1$ g m^{-3}, so that this effect is assumed to be relevant only for $LWC < 0.1$ g m^{-3}.

In Fig. 4a, the time series of D_{50} is plotted along with the error bars given by the fitting procedure. The fitting procedure worked well for higher *LWC* values, where the error bars are small and the calculated D_{50} consistently is around 100 nm. For less dense clouds D_{50} increases up to 700 nm. These high values can be explained by the fact that 1-h averages were used for the fitting procedure. In the following only D_{50} are considered with a calculated error less than 10 nm (in addition to the criteria of *LWC* 15th percentile).

In Fig. 4c the diameters of 25%, 50% and 75% activation (D_{25}, D_{50} and D_{75}) are shown which give an impression of the activation steepness. D_{25} and D_{75} were again calculated from the fitting function. There are two possible reasons why the activation curve is not a step function: either due to the variability of the supersaturation or due to an external mixture of the aerosol. The first assumption is more likely because the latter is refuted by hygroscopicity measurements at this site (see below).

Assuming a similar chemical composition of the particles over the measured size range and thus internal mixture with respect to its activation behavior, the width of the activation curve, i.e. the difference between 75% activation and 25%, gives a measure of the variability in supersaturation. In general the observed activation diameters are similar to those of other authors (Table 2), who reported D_{50} values between 0.09 and 0.31 µm. Generally, activation diameters from sites close to emission sources appear to be higher than in areas with lower emissions. There are two possible reasons for this: on the one hand, the aerosol is usually more hydrophobic at sites close to emission sources, and on the other hand, the higher particle number concentration may reduce the maximum supersaturation of the cloud, both resulting in an increase of D_{50}. Similar low D_{50} values down to 70 nm were observed in less polluted air masses (Schwarzenboeck et al., 2000). Generally the effective radii observed at the JFJ (about 10 µm) are larger than at the other sites.

3.3. Dependence of D_{50} on other parameters

From Fig. 4a it is concluded that there is a correlation between the *LWC* of the cloud and the calculated D_{50}. This is shown in more detail in Fig. 5. For low *LWC* up to 0.25 g m^{-3} D_{50} decreases with increasing *LWC*. Above this value D_{50} stabilizes around 100 nm, where other parameters seem to influence the value of D_{50}.

To check if the accumulation mode particle number concentration influences D_{50}, the SMPS spectra were integrated over the 100–800 nm particle diameter range. Figure 6 shows D_{50} as a function of the accumulation mode number concentration again for stable cloud conditions (*LWC* 15th percentile > 0.02 g m^{-3}). For accumulation mode particle concentrations $N_{tot,D_p>100} < 100$ cm^{-3}, D_{50} appears to be lower, while above $N_{tot,D_p>100} \approx 100$ cm^{-3} the activation diameter stays more or less constant around 100 nm. As a result it is concluded that for low number concentrations, particles with diameters smaller than 100 nm are also activated, pointing to a higher supersaturation in those cases (see Section 3.4). Apparently, the low particle number concentration results in a less efficient flux of the available water to the particles resulting in a higher supersaturation.

LWC and N_{tot} also have an influence on the effective droplet radius R_{eff}. This parameter is defined in eq. (2) and is a mean radius of the cloud droplet size distribution, which is often used to parameterize cloud optical properties (e.g. optical

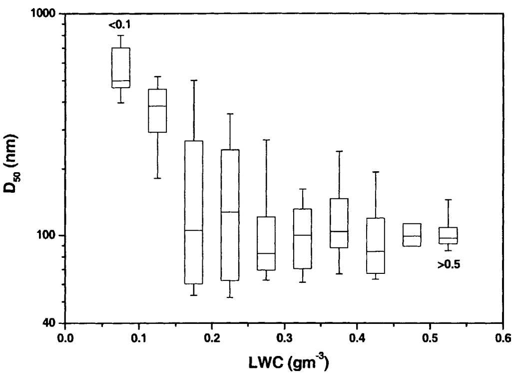

Fig. 5. Activation diameter (10th, 25th, median, 75th, 90th percentile) versus *LWC* classes for the whole measuring campaign for stable cloud times (*LWC* 15th percentile > 0.02 g m^{-3}).

Table 2. *Averaged aerosol and cloud properties (droplet number concentration N_D, for other description see text) from JFJ in comparison with examples from literature*

LWC (g m^{-3})	N_{tot} (cm^{-3})	$N_{tot,D_p>100\,nm}$ (cm^{-3})	N_{int} (cm^{-3})	N_D (cm^{-3})	R_{eff} (µm)	D_{25} (µm)	D_{50} (µm)	D_{75} (µm)	F_N	Reference
0.1–0.2	1731	424		326	5–8[a)]	0.09	0.11	0.17	0.73[b)]	Hallberg et al. (1994)
			500–1000		4.5–5.5[a)]		0.14		0.17–0.45[c)]	Schwarzenboeck et al. (2000)
	282	102	215	112	9	0.16	0.28	0.39	0.46	This paper
0.2–0.3	231	95	130	125	10	0.07	0.15	0.23	0.72	This paper
0.3–0.4		190		180	6.7		0.10		0.88[d)]	Martinsson et al. (1999)
		2500		1500	4.05		0.15		0.98[d)]	Martinsson et al. (1999)
	379	198	217	185	10	0.08	0.12	0.15	0.76	This paper
0.4–0.5	2742	813		289	5–10[a)]	0.24	0.28	0.33	0.18[b)]	Hallberg et al. (1994)
	2671	1180		327	6–9[a)]	0.24	0.31	0.40	0.12[b)]	Hallberg et al. (1994)
			500–1000		5.5–6.5[a)]		0.07–0.12		0.16–0.55[c)]	Schwarzenboeck et al. (2000)
	331	162	182	190	10.4	0.08	0.10	0.13	0.81	This paper
>0.5		250		190	8.65		0.13		0.93[d)]	Martinsson et al. (1999)
		650		380	7.9		0.14		0.93[d)]	Martinsson et al. (1999)
		400		300	7.3		0.12		0.90[d)]	Martinsson et al. (1999)
	595	315	278	416	9.6	0.08	0.10	0.13	0.84	This paper
	2600	1023					0.09–0.22			Svenningsson et al. (1997)

The activated fraction of the aerosol F_N was calculated for particles with $100 < D_p < 800$ nm if not mentioned otherwise.
[a)] Estimated from the diameter of mean volume (D_{VMD}); $R_{eff} \cong D_{VMD}/2$.
[b)] $100 < D_p < 1000$ nm.
[c)] $25 < D_p < 850$ nm.
[d)] $230 < D_p < 660$ nm.

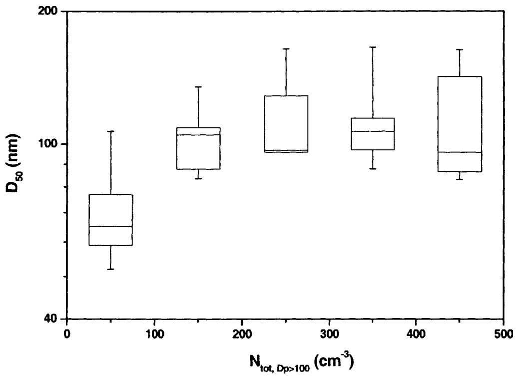

Fig. 6. Diameter of 50% activation (10th, 25th, median, 75th, 90th percentile) plotted versus total number concentration of particles with a diameter greater than 100 nm. Only activation diameters for 15th percentile of *LWC* higher than 0.02 g m^{-3} were used for calculation.

thickness). The relation between the accumulation mode particle concentration $N_{tot,D_p>100}$ and R_{eff} (measured by the FSSP) for different *LWC* classes is plotted in Fig. 7. The theoretical description of the relationship is given by:

$$LWC = \rho_w N_{tot,D_p>100} \frac{4\pi}{3} R_{eff}^3, \tag{8}$$

in which an activation of all particles larger than 100 nm is assumed. The lines in Fig. 7 are the results of fitting three *LWC* classes with this model. It can be seen that above the 'critical' value of $N_{tot,D_p>100} \approx 100\ cm^{-3}$ (marked with a dashed

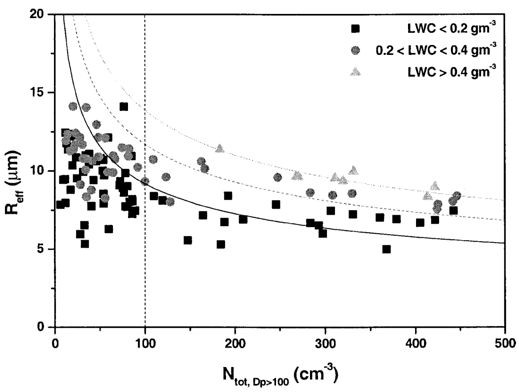

Fig. 7. Effective droplet radius versus total number concentration of particles with diameters greater than 100 nm for three *LWC* classes, along with the fit functions from eq. (8).

line) the measurements are well described by eq. (8). The droplet effective radius decreases with increasing $N_{tot,D_p>100}$ and thus confirms the expected microphysical relation predicted by the Twomey effect, in agreement with observations by others (Raga and Jonas, 1993). For lower values of $N_{tot,D_p>100}$ smaller R_{eff} were found than predicted by this model. Most probably particles with $D_p < 100$ nm also become activated in these cases, as already indicated by Fig. 6. It should be mentioned that such an analysis is a strong simplification of the multidimensional activation process in the real atmosphere. Nevertheless, it is believed that it delivers valuable information that may be used as input in future models.

3.4. *Critical supersaturation for the JFJ aerosol*

During another intensive measuring campaign at the JFJ station (CLACE: Cloud and Aerosol Characterization Experiment in the Free Troposphere, February/March 2000), hygroscopic growth measurements under ambient temperatures (-10 °C) were performed with a hygroscopicity tandem differential mobility analyzer (H-TDMA) (Weingartner et al., 2002). In addition to the growth factors for three different dry particle diameters ($D_0 = 50$, 100, 250 nm) at $RH = 85\%$, several humidograms between $10 < RH < 85\%$ were also measured. These data pairs (D_{wet}/D_0 as a function of RH) were fitted with a modified Köhler model as described by Brechtel and Kreidenweis (2000a, b). By fitting the humidograms with the model the chemical composition was parameterized, which allowed the critical supersaturation S_c required for particle activation to be determined. The critical supersaturation S_c was also calculated for pure ammonium sulfate particles at -10 and 20 °C (Fig. 8). For a $D_{50} =$ 100 nm Fig. 8 yields a critical supersaturation of about 0.2%.

It can be seen that the JFJ aerosol particles require a slightly higher supersaturation compared to the value of S_c required to activate pure ammonium sulfate particles. The fact that the JFJ aerosol exhibits similar behavior to ammonium sulfate particles is reasonable in the light of the measured chemical composition. The concentration of major ions in the summer of 1998 and 2000 are given in Table 3. During the 1998 summer campaign additional chemical parameters were analyzed

(Krivacsy et al., 2001). Based on the fact that the fractional composition of the major inorganic ions (sulfate, ammonium and nitrate) was found to be similar for both years (50–60%), it is reasonable to assume that the total soluble fraction of the accumulation mode aerosol at the JFJ under summer conditions is about 80%.

4. Conclusions

Aerosol size distributions of the total and interstitial aerosol were measured at the high-alpine station JFJ during a 3-week campaign in summer 2000. During cloudless periods identical size spectra were observed for the different inlet types. When clouds were present, the complete accumulation mode was usually activated. Good agreement was found between droplet number concentrations derived from the SMPS aerosol size distributions and those measured by the FSSP. From the measured aerosol and droplet size distributions the scavenging ratio for each particle diameter and the 50% activation diameter (D_{50}) was calculated over the whole campaign. The D_{50} was found to be influenced by the available amount of liquid water and accumulation mode number concentration below a certain threshold. Above this threshold other parameters appeared to influence the D_{50} more effectively. A decrease of the effective drop size R_{eff} with increasing number concentration of the accumulation mode particles gave experimental evidence for the microphysical part of the Twomey effect. Furthermore, a modified Köhler model was used to study the critical supersaturation for the JFJ aerosol. From the derived supersaturation curve and the calculated D_{50}, ambient supersaturations were determined. The reasonable value of $S_c = 0.2\%$ for a D_{50} of 100 nm is obtained.

5. Acknowledgements

We thank the International Foundation High Altitude Research Stations Jungfraujoch and Gornergrat (HFSJG) which made it possible for us to carry out our experiments at the High Altitude Research Station at Jungfraujoch. The financial support of MeteoSwiss (Global Atmosphere Watch) is highly appreciated. We also thank Stephan Nyeki for editing the manuscript.

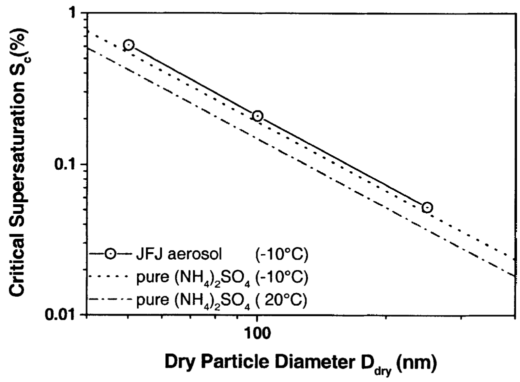

Fig. 8. Critical supersaturation for JFJ aerosol at ambient temperature, and ammonium sulfate at −10 and 20 °C calculated with the model from (Brechtel and Kreidenweis, 2000a).

Table 3. *Amount of sulfate, ammonium, nitrate, water-soluble organic substances (WSOS) and water insoluble organic substances (WINSOS) given as absolute values and as fraction of the fine particulate matter for the summer campaigns 1998 and 2000*

	Summer 1998[a]		Summer 2000	
	($\mu g\, m^{-3}$)	(%)	($\mu g\, m^{-3}$)	(%)
TSP	6.62[b]		3.53[b]	
$PM_{2.5}$	3.12	100	1.66[c]	100
Sulfate	1.07	34.3	0.42	25.5
Ammonium	0.34	10.9	0.12	7.0
Nitrate	0.30	9.6	0.25	14.9
WINSOS	0.64[d]	20.4		
WSOS	1.20[e]	38.4		

[a] Krivacsy et al. (2001).
[b] Source: Swiss Agency for the Environment, Forests and Landscape (BUWAL)/Swiss National Monitoring Network for Air Pollutants (NABEL).
[c] Assuming the same TSP/$PM_{2.5}$ ratio for summer 2000 as for summer 1998 (Krivacsy et al., 2001).
[d] Applying a correction factor of 1.2 to calculate WINSOS from the water insoluble organic carbon (WINSOC).
[e] Applying a correction factor of 1.9 to calculate WSOS from the water-soluble organic carbon (WSOC) as experimentally determined by Krivacsy et al. (2001).

REFERENCES

Arends, B. G., Kos, G. P. A., Wobrock, W., Schell, D., Noone, K., Fuzzi, S. and Pahl, S. 1992. Comparison of techniques for measurements of fog liquid water content. *Tellus* **44B**, 604–611.

Baltensperger, U., Schwikowski, M., Jost, D. T., Nyeki, S., Gäggeler, H. W. and Poulida, O. 1998. Scavenging of atmospheric constituents in mixed phase clouds at the high-alpine site Jungfraujoch, Part I. Basic concept and aerosol scavenging by clouds. *Atmos. Environ.* **32**, 3975–3983.

Baltensperger, U., Gäggeler, H. W., Jost, D. T., Lugauer, M., Schwikowski, M., Weingartner, E. and Seibert, P. 1997. Aerosol climatology at the high-alpine site Jungfraujoch, Switzerland. *J. Geophys. Res.* **102**, 19,707–19,715.

Baumgardner, D. and Spowart, M. 1990. Evaluation of the forward scattering spectrometer probe, Part III. Time response and laser inhomogeneity limitations. *J. Atmos. Oceanic Technol.* **7**, 666–672.

Baumgardner, D., Strapp, W. and Dye, J. E. 1985. Evaluation of the forward scattering spectrometer probe, Part II. Corrections for coincidence and dead-time losses. *J. Atmos. Oceanic Technol.* **2**, 626–632.

Brechtel, F. J. and Kreidenweis, S. M. 2000a. Predicting particle critical supersaturation from hygroscopic growth measurements in the humidified TDMA, Part I. Theory and sensitivity studies. *J. Atmos. Sci.* **57**, 1854–1871.

Brechtel, F. J. and Kreidenweis, S. M. 2000b. Predicting particle critical supersaturation from hygroscopic growth measurements in the humidified TDMA, Part II. Laboratory and ambient studies. *J. Atmos. Sci.* **57**, 1872–1887.

Brenguier, J.-L. 1989. Coincidence and dead-time corrections for particle counters, Part I. A general mathematical formalism. *J. Atmos. Oceanic Technol.* **6**, 575–584.

Cerni, T. A. 1983. Determination of the size and concentration of cloud drops with an FSSP. *J. Climate Appl. Meteorol.* **22**, 1346–1355.

Choularton, T. W., Consterdine, I. E., Gardiner, B. A., Gay, M., Hill, M. K., Latham, J. and Stromberg, I. M. 1986. Field studies of the optical and microphysical characteristics of clouds enveloping Great Dun Fell. *Q. J. R. Meteorol. Soc.* **112**, 131–148.

Choularton, T. W., Colvile, R. N., Bower, K. N., Gallagher, M. W., Wells, M. and coauthors 1997. The Great Dun Fell Cloud Experiment 1993: an overview. *Atmos. Environ.* **31**, 2393–2405.

Dye, J. E. and Baumgardner, D. 1984. Evaluation of the forward scattering spectrometer probe, Part I. Electronic and optical studies. *J. Atmos. Oceanic Technol.* **1**, 329–344.

Gerber, H. 1991. Direct measurement of suspended particulate volume concentration and far-infrared extinction coefficient with a laser-diffraction instrument. *Appl. Opt.* **30**, 4824–4831.

Gillani, N. V., Schwartz, S. E., Leaitch, W. R., Strapp, J. W. and Isaac, G. A. 1995. Field observations in continental stratiform clouds:Partitioning of cloud particles between droplets and unactivated aerosols. *J. Geophys. Res.* **100**, 18,687–18,706.

Hallberg, A., Noone, K., Ogren, J. A., Svenningsson, B., Flossmann, A. I., Wiedensohler, A., Hansson, H. C., Heintzenberg, J., Anderson, T., Arends, B. G. and Maser, R. 1994. Phase partitioning of aerosol particles in clouds at Kleiner Feldberg. *J. Atmos. Chem.* **19**, 107–127.

IPCC 2001. *Climate Change 2001: The Scientific Basis* (eds. J. T. Houghton, Y. Ding, D. J. Griggs, M. Noguer, P. J. van der Linden, H. X. Dai, K. Maskell and C. A. Johnson). Cambridge University Press, Cambridge, 881 pp.

Knollenberg, R. G. 1981. Techniques for probing cloud microstructure. In: *Clouds, their formation, optical properties and effects* (eds. P. V. Hobbs and A. Deepak). Academic Press, Inc., New York, pp. 15–91.

Krivacsy, Z., Gelencser, A., Kiss, G., Meszaros, E., Molnar, A., Hoffer, A., Meszaros, T., Sarvari, Z., Temesi, D., Varga, B., Baltensperger, U., Nyeki, S. and Weingartner, E. 2001. Study on the chemical character of water soluble organic compounds in the fine atmospheric aerosol at the Jungfraujoch. *J. Atmos. Chem.* **39**, 235–259.

Leaitch, W. R., Banic, C. M., Isaac, G. A., Couture, M. D., Liu, P. S. K., Gultepe, I., Li, S. M., Kleinman, L., Daum, P. H. and MacPherson, J. I. 1996. Physical and chemical observations in marine stratus during the 1993 North Atlantic Regional Experiment: factors controlling cloud droplet number concentrations. *J. Geophys. Res.* **101**, 29,123–29,135.

Maenhaut, W., Hillamo, R., Mäkelä, T., Jaffrezo, J. L., Bergin, M. H. and Davidson, C. I. 1996. A new cascade impactor for aerosol sampling with subsequent PIXE analysis. *Nucl. Instr. and Meth. in Phys. Res. B.* **109**, 482–487.

Martinsson, B. G., Frank, G., Cederfelt, S. I., Swietlicki, E., Berg, O. H., Zhou, J. C., Bower, K. N., Bradbury, C., Birmili, W., Stratmann, F., Wendisch, M., Wiedensohler, A. and Yuskiewicz, B. A. 1999. Droplet nucleation and growth in orographic clouds in relation to the aerosol population. *Atmos. Res.* **50**, 289–315.

Nyeki, S., Baltensperger, U., Colbeck, I., Jost, D. T., Weingartner, E. and Gäggeler, H. W. 1998. The Jungfraujoch high-alpine research station (3454 m) as a background clean continental site for the measurement of aerosol parameters. *J. Geophys. Res.* **103**, 6097–6107.

Onasch, T. B., Siefert, R. L., Brooks, S. D., Prenni, A. J., Murray, B., Wilson, M. A. and Tolbert, M. A. 1999. Infrared spectroscopic study of the deliquescence and efflorescence of ammonium sulfate aerosol as a function of temperature. *J. Geophys. Res.* **104**, 21,317–21,326.

Pruppacher, H. R. and Klett, J. D. 1980. *Microphysics of clouds and precipitation*. Dordrecht, Boston, London, 714 pp.

Raga, G. B. and Jonas, P. R. 1993. On the link between cloud-top radiative properties and sub-cloud aerosol concentrations. *Q. J. R. Meteorol. Soc.* **119**, 1419–1425.

Schwarzenboeck, A., Heintzenberg, J. and Mertes, S. 2000. Incorporation of aerosol particles between 25 and 850 nm into cloud elements: measurements with a new complementary sampling system. *Atmos. Res.* **52**, 241–260.

Svenningsson, B., Hansson, H. C., Martinsson, B., Wiedensohler, A., Swietlicki, E., Cederfelt, S. I., Wendisch, M., Bower, K. N., Choularton, T. W. and Colvile, R. N. 1997. Cloud droplet nucleation scavenging in relation to the size and hygroscopic behaviour of aerosol particles. *Atmos. Environ.* **31**, 2463–2475.

Twomey, S. 1974. Pollution and the planetary albedo. *Atmos. Environ.* **8**, 1251–1256.

Twomey, S. 1977. The influence of pollution on the short-wave albedo of clouds. *J. Atmos. Sci.* **34**, 1149–1152.

Weingartner, E., Nyeki, S. and Baltensperger, U. 1999. Seasonal and diurnal variation of the aerosol size distributions ($10 < D < 750$ nm) at a high-alpine site (Jungfraujoch 3580 m asl). *J. Geophys. Res.* **104**, 26,809–26,820.

Weingartner, E., Gysel, M. and Baltensperger, U. 2002. Hygroscopicity of aerosol particles at low temperatures, 1. New low temperature H-TDMA system: setup and first applications. *Environ. Sci. Technol.*, in press.

Wendisch, M. 1998. A quantitative comparison of ground-based FSSP and PVM measurements. *J. Atmos. Oceanic Technol.* **15**, 887–900.

Wendisch, M., Keil, A. and Korolev, A. V. 1996. FSSP characterization with monodisperse water droplets. *J. Atmos. Oceanic Technol.* **13**, 1152–1165.

Wendisch, M., Garrett, T. J. and Strapp, J. W. 2001. Wind tunnel tests of the airborne PVM-100A response to large drops. *J. Atmos. Oceanic Technol.*, in press.

Wendisch, M., Mertes, S., Heintzenberg, J., Wiedensohler, A., Schell, D., Wobrock, W., Frank, G., Martinsson, B., Fuzzi, S., Orsi, G., Kos, G. P. A. and Berner, A. 1998. Drop size distribution and LWC in Po Valley fog. *Contr. Atmos. Phys.* **71**, 87–100.